Supporting Information for "Implications of Rewiring Bacterial Quorum Sensing"

Eric L. Haseltine and Frances H. Arnold*
Division of Chemistry & Chemical Engineering 210-41
California Institute of Technology, Pasadena, CA 91125
*e-mail:frances@cheme.caltech.edu

November 15, 2007

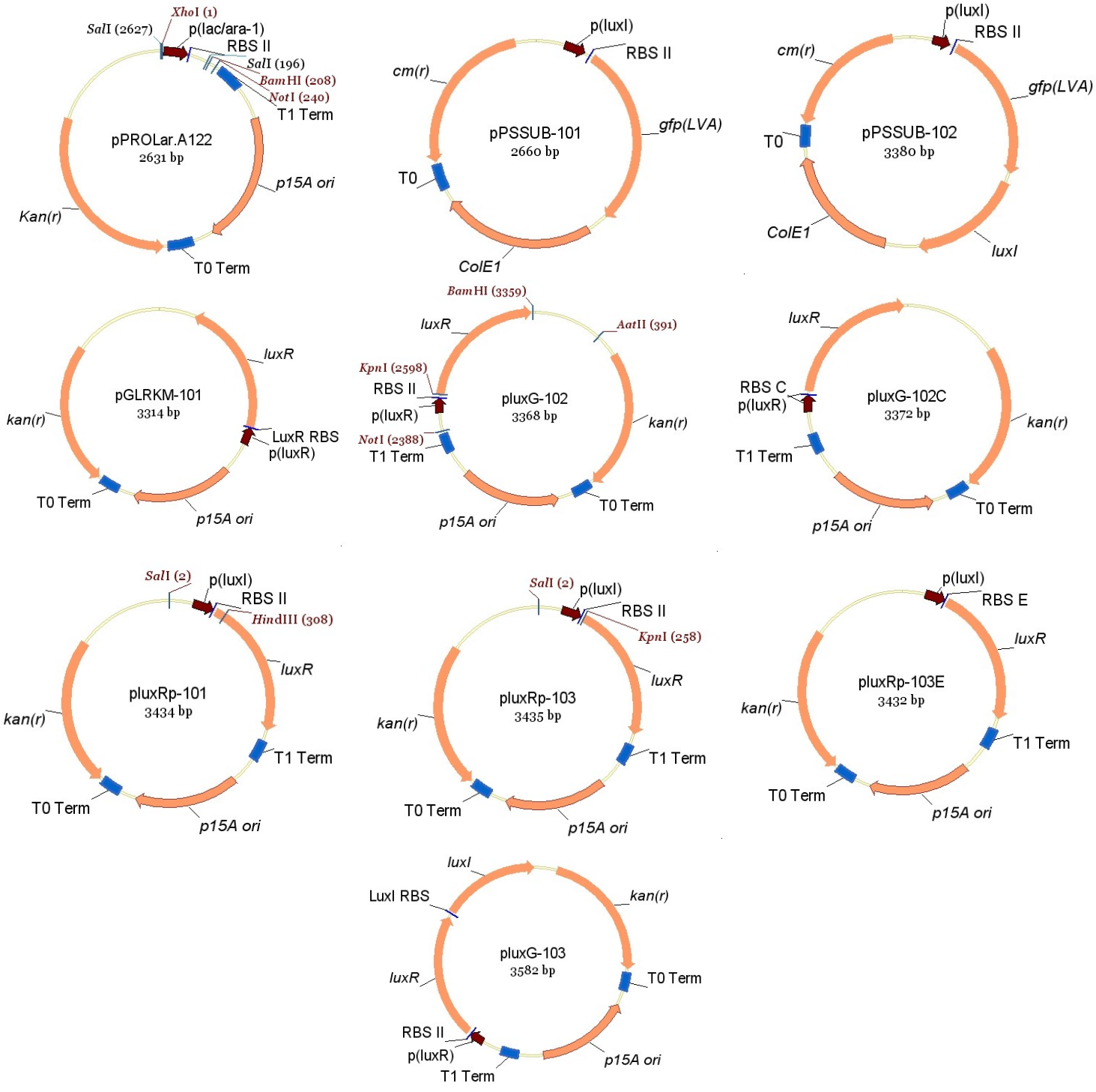

Figure S1: Plasmids used in this study.

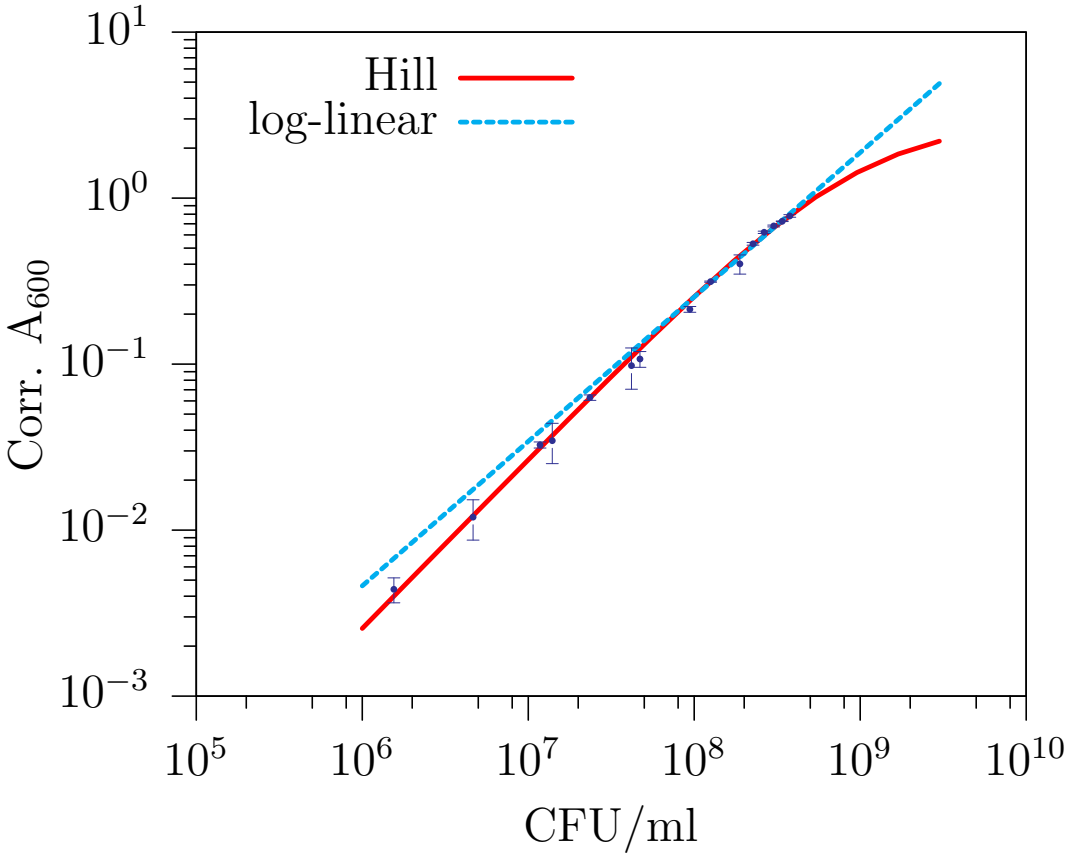

Figure S2: A Hill function accurately fits the relationship between corrected absorbance and CFU/ml in LBM medium. A log-linear fit of the form $\log_{10}(\mathrm{A}_{600} - c_3^l) = c_1^l \log_{10}(r) + c_2^l$ is shown for comparison. The small standard deviations of the experimental data at high absorbances make this log-linear fit less predictive than the Hill function.

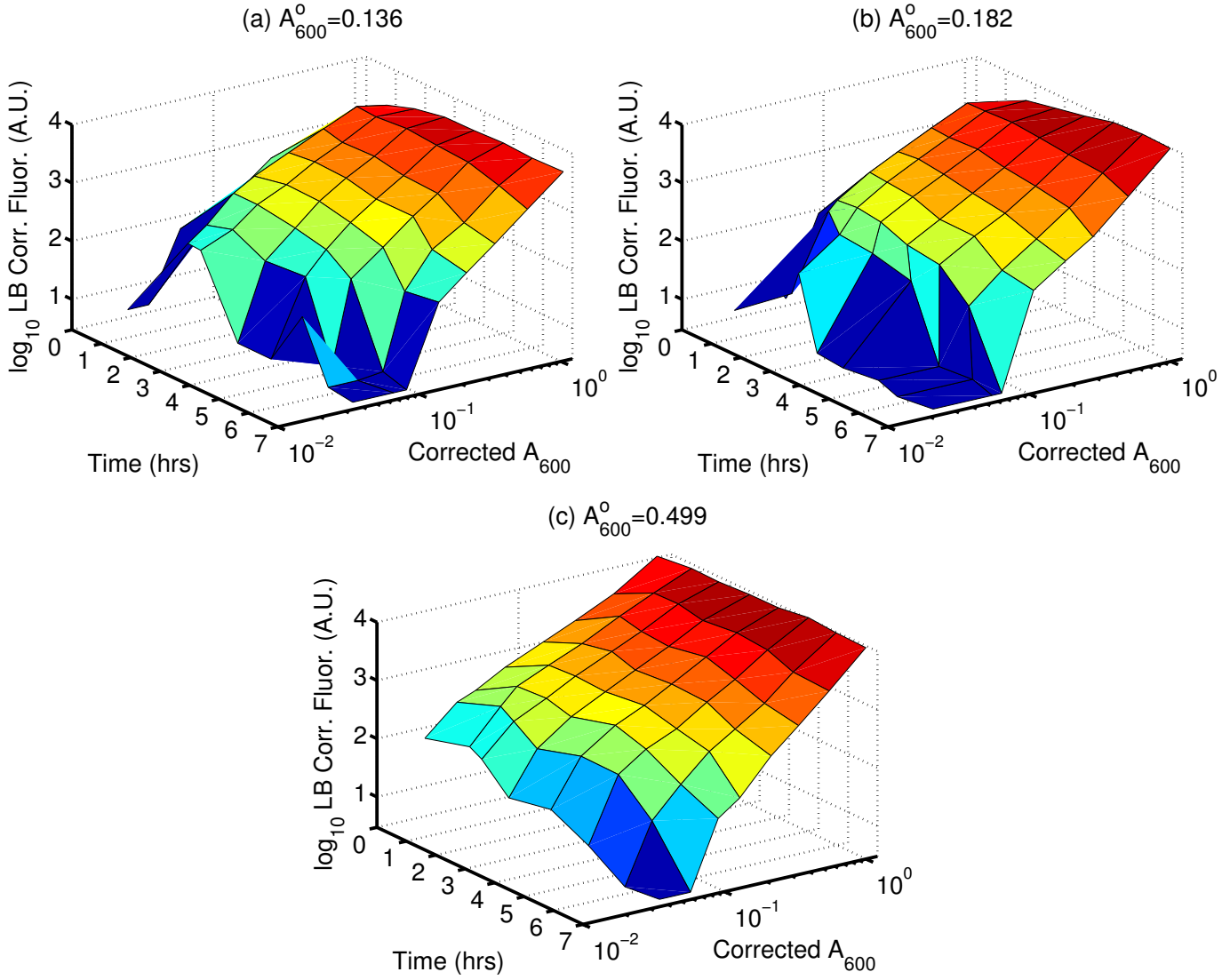

Figure S3: Periodic dilution results for network architecture c, pluxRp-101 and pPSSUB-102. This figure shows the corrected absorbance and fluorescence dynamics over the duration of the periodic dilution experiment. A^o_{600} is the initial absorbance of the overnight culture used to start the periodic dilution experiment. The system exhibited the same fluorescence trend regardless of the initial condition: an initial burst followed by a gradual decay. Each plot uses the same shading to highlight differences in the measured fluorescence values.

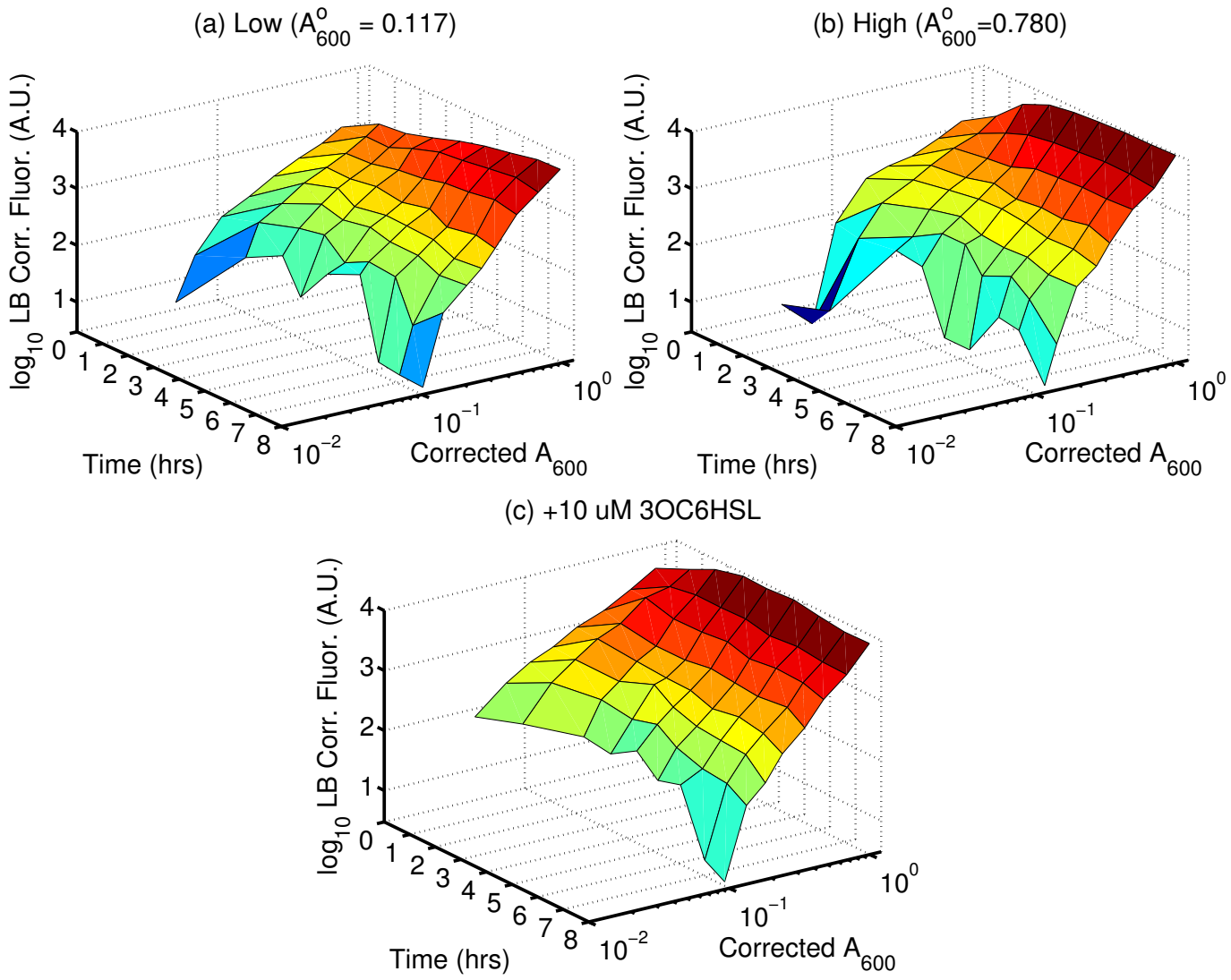

Figure S4: Periodic dilution results for network architecture b, pluxG-102C and pPSSUB-102. This figure shows the corrected absorbance and fluorescence dynamics over the duration of the periodic dilution experiment. A^o_{600} is the initial absorbance of the overnight culture used to start the periodic dilution experiment. +10 μM 3OC6HSL indicates that the overnight culture was induced with 10 μM 3OC6HSL. Each plot uses the same shading to highlight differences in the measured fluorescence values.

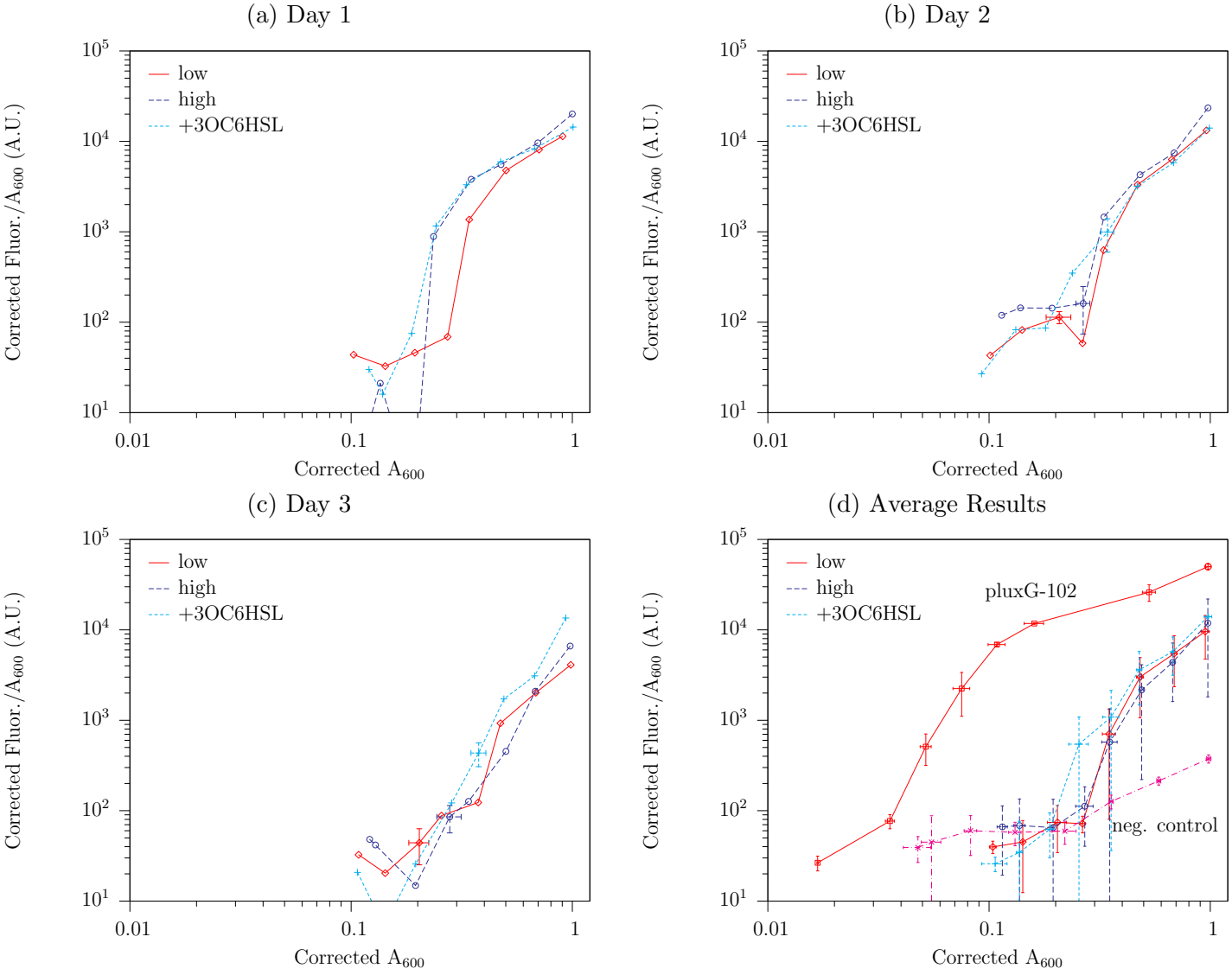

Figure S5: Individual periodic dilution experiments for testing of architecture b (pluxG-102C and pPSSUB-102) for bi-stability. Here, initial cultures were either grown to a **low** absorbance ($A_{600} < 0.2$), grown to a **high** absorbance ($A_{600} > 0.7$), or dosed with 10 μM **3OC6HSL**. In each experiment, these different initial conditions led to very similar steady-state profiles. The variation in the steady-state data from day to day, plots (a-c), led to the variability in the average results, plot (d).

(a) - Figure 3 and Figure 5

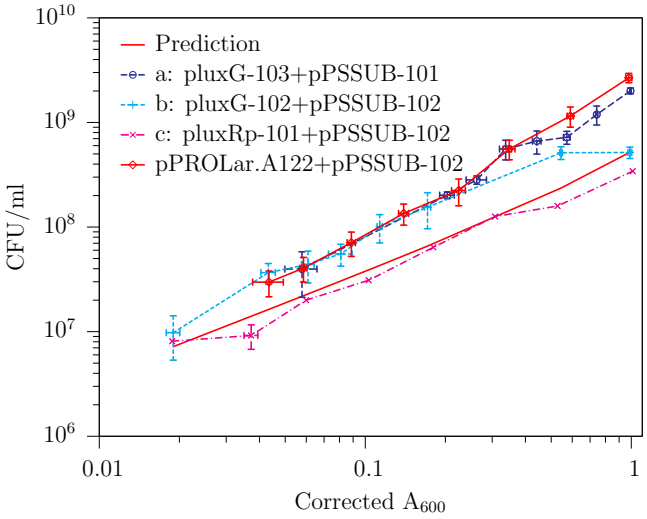

(b) - Figure 3: pluxRp-103E and pPSSUB-102

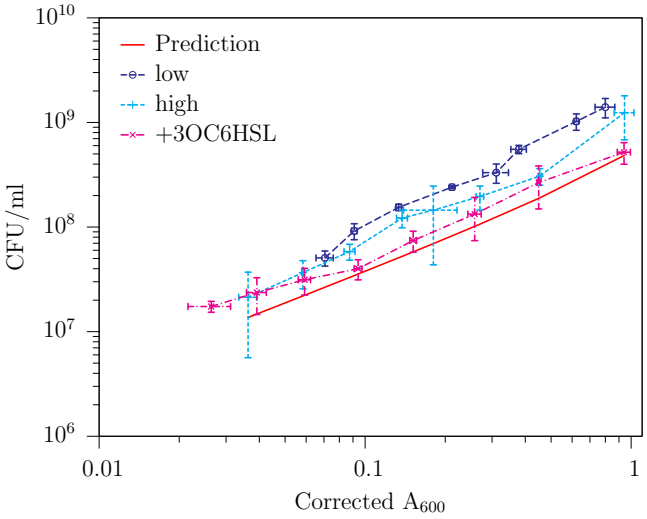

(c) - Figure 7: pluxG-102C and pPSSUB-102

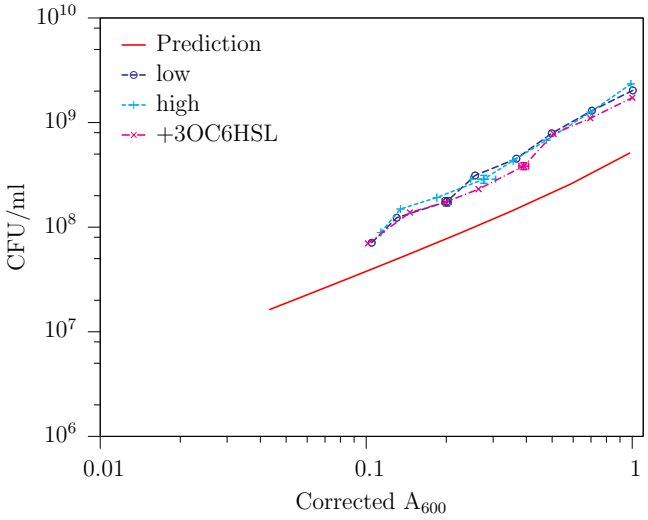

Figure S6: Cell viability for the periodic dilution experiments as determined by serial dilution and plating. Each plot corresponds to a periodic dilution experiment in the main text as noted.

Primer	Sequence	Constructed Plasmid
5-G-NotI	aagcgcggccgcctcgtaagccatttccgctcg	pluxG-102, pluxG-102C
3-XhoI-luxR	gaactctcgaggatcccgtacttaatttttaaagtatgg	pluxG-102
5-G2-lux	cttgcgacaaacaatattaaagaggagaaaggtacccatg	pluxG-102
3-G2-lux	ctcctctttaatattgtttgtcgcaagttttgcgtg	pluxG-102
3-KpnI-GC	ctatgaggtaccggtctgtttccttacctattgtttgtcgcaagttttg	pluxG-102C
5-AatII-luxI	ctagaggacgtcttaatttaagactgctttttttaaactg	pluxG-103
5-Rseq	ttcatacggctaacaatggcttcg	pluxG-103
5-SalI-plux	gaactgtcgacccctcttacgtgccgatcaacgtctc	pluxRp-101
3-pluxC	catttatgtttttcatgcttaatttctcctcttttatcaccg	pluxRp-101
5-luxRC	gagaaattaagcatgaaaaacataaatgccgacgacac	pluxRp-101
5-seq	catagccgaatagcctctccac	pluxRp-101
5-Rp-SalI	agcaatcacctatgaactgtcg	pluxRp-103, pluxRp-103E
3-HindIII-luxRa	gcttctacaagctttaattttattaattattctgtatg	pluxRp-103
5-Rp3	gataaaagaggagaaggtaccatgaaaaacataaatg	pluxRp-103
3-Rp3	catttatgtttttcatggtaccttctcctcttttatc	pluxRp-103
3-KpnI-RpE	ctatgaggtaccaaccggtttcctcaccgccagaggtattcgac	pluxRp-103E

Table S1: Primers used in this study.

$2\mathrm{R} + 2\mathrm{A} \overset{K_1}{\rightleftharpoons} \mathrm{R}^*$	r_1	Transcription Factor Binding
$\mathrm{R}^* + \mathrm{P}_0 \overset{K_2}{\rightleftharpoons} \mathrm{P}_1$	r_2	
$\mathrm{R}, \mathrm{A}, \mathrm{G} \overset{k_5, k_6, k_7}{\longrightarrow}$ degraded	r_5, r_6, r_7	Degradation
$\mathrm{C} \overset{k_9}{\longrightarrow} 2\mathrm{C}$	$\mathrm{r}_9 = \mathrm{k}_9\mathrm{c}\left(1 - \frac{\mathrm{c}}{\mathrm{c}_{\max}}\right)$	Cell growth (logistic)
$\mathrm{P}_0 \overset{k_4}{\longrightarrow} \mathrm{P}_0 + \mathrm{n_a A} + \mathrm{n_g G}$	r_4	Transcription & Translation
$\mathrm{P}_1 \overset{k_3}{\longrightarrow} \mathrm{P}_1 + \mathrm{n_a A} + \mathrm{n_g G}$	r_3	
$\mathrm{Q}_0 \overset{k_8}{\longrightarrow} \mathrm{Q}_0 + \mathrm{R}$	r_8	

Table S2: Kinetic mechanism used to model the behaviors of network architecture b. G, C, and Q_0 refer to green fluorescent protein, bacterial cells, and the DNA encoding constitutive expression, respectively.

S1 Derivation of the Quorum-Sensing Mathematical Model

In this section, we derive the mass balances used to construct the quorum-sensing mathematical model. We consider only architecture b, in which *luxR* is constitutively expressed and *luxI* and *gfplva* are under the control of the *p(luxI)* promoter. The other two configurations can be similarly derived.

Given the kinetic mechanism of Table S2, we can write mass balances for each of the species of interest

$$\frac{d(c_A V)}{dt} = \left(-2r_1 + n_a(r_3 + r_4)\right) V_c - r_6 V \tag{1a}$$

$$\frac{d(c_R V_c)}{dt} = \left(-2r_1 + r_8 - r_5\right) V_c \tag{1b}$$

$$\frac{d(c_{R^*} V_c)}{dt} = \left(r_1 - r_2\right) V_c \tag{1c}$$

$$\frac{dc_{P_0}}{dt} = -r_2 \tag{1d}$$

$$\frac{dc_{P_1}}{dt} = r_2 \tag{1e}$$

$$\frac{d(c_G V_c)}{dt} = \left(n_G(r_3 + r_4) - r_7\right) V_c \tag{1f}$$

$$\frac{d(c_c V)}{dt} = r_9 V \tag{1g}$$

in which

- V = reactor volume,

Parameter	Initial Value	Reference	Revised Value
K_1	10. nM^{-1}		50. nM^{-1}
K_2	0.01 nM^{-1}	[8]	
k_3	20. hr^{-1}	[4]	
k_4	4.05×10^{-6} hr^{-1}	[4]	0.1 hr^{-1}
k_5	1.386 hr^{-1}	[3]	
k_6	0.0289 hr^{-1}	[5]	
k_7	1.0397 hr^{-1}	[1]	
k_8	0.4819 hr^{-1}		0.0723 hr^{-1}
n_A	$1. \times 10^3$		
n_G	1.		
c_{P_T}	41.5 nM		
c_{Q_T}	41.5 nM		
V	5. ml		
V_{one}	$10.^{-15}$ l	[2]	
k_G	1. nM^{-1}		50. nM^{-1}
f_{bgd}	0		-150

Table S3: Parameters used for simulation of the quorum-sensing models. Initial values for parameters were obtained from the literature when possible. The revised values reflect adjustments made to parameters to fit the experimental results for the shuffled architectures.

- V_{one} = volume of one cell,
- V_c = total intracellular volume = $c_c V V_{\text{one}}$, and
- $c_{c,\max}$ = max cell density.

Here, we assume that cell replication maintains a constant plasmid concentration. We assume that fluorescence (f) is proportional to the GFPLVA concentration (c_G) plus a scaling factor f_{bgd}, i.e.,

$$f = k_G c_G + f_{\text{bgd}} \tag{2}$$

A list of parameters used in this paper are presented in Table S3. Parameters such as k_9 that do not affect the steady state are not reported in this table.

Assuming that reactions one and two (r_1 and r_2) are at equilibrium, we obtain the following reduced model:

$$\frac{d(c_A V)}{dt} + 2\left(\frac{d(c_{R^*} V_c)}{dt} + V_c \frac{dc_{P_1}}{dt}\right) = \left(n_a(r_3 + r_4)\right) V_c - r_6 V \tag{3a}$$

$$\frac{d(c_R V_c)}{dt} + 2\left(\frac{d(c_{R^*} V_c)}{dt} + V_c \frac{dc_{P_1}}{dt}\right) = (r_8 - r_5)\, V_c \tag{3b}$$

$$K_1 = \frac{c_{R^*}}{c_A c_R} \tag{3c}$$

$$K_2 = \frac{c_{P_1}}{c_{P_0} c_{R^*}} \tag{3d}$$

$$c_{P_T} = c_{P_0} + c_{P_1} \tag{3e}$$

$$\frac{d(c_G V_c)}{dt} = \left(n_G(r_3 + r_4) - r_7\right) V_c \tag{3f}$$

$$\frac{d(c_c V)}{dt} = r_9 V \tag{3g}$$

in which c_{P_T} is the total plasmid concentration per cell.

By setting the derivatives of equation (3), one can solve for the steady states of the system to yield:

$$0 = -k_6\alpha c_A^2 + (k_3\alpha\beta - k_6)\, c_A + k_4\beta \tag{4a}$$

$$\alpha = K_1K_2 \tag{4b}$$

$$\beta = n_a V_c c_{c,\max} c_{P_T} \tag{4c}$$

$$c_G = \frac{n_g c_{P_T}}{k_7} \frac{(k_4 + K_1K_2k_3c_Ac_R)}{(1 + K_1K_2c_Ac_R)} \tag{4d}$$

Equation (4) indicates that the steady-state concentration of the 3OC6HSL signalling molecule is a quadratic function.

In a similar fashion, one can solve for the steady states of network architecture a

$$c_A = \frac{n_a V_c k_8}{k_6} c_{c,\max} \tag{5a}$$

$$c_R = \frac{k_8}{k_5} \tag{5b}$$

$$c_{P_T} = c_{\mathrm{P}_0} + c_{\mathrm{P}_1} \tag{5c}$$

$$c_G = \frac{n_g c_{P_T}}{k_7} \frac{(k_4 + K_1K_2k_3c_Ac_R)}{(1 + K_1K_2c_Ac_R)} \tag{5d}$$

and network architecture c

$$0 = -k_6\alpha c_A^3 + k_3\alpha\beta c_A^2 - k_6 c_A + k_4\beta \tag{6a}$$

$$\alpha = K_1K_2 \tag{6b}$$

$$\beta = n_a V_c c_{c,\max} c_{P_T} \tag{6c}$$

$$c_G = \frac{n_g c_{P_T}}{k_7} \frac{(k_4 + K_1K_2k_3c_Ac_R)}{(1 + K_1K_2c_Ac_R)} \tag{6d}$$

Equations (5) and (6) indicate that the steady-state concentration of the 3OC6HSL signalling molecule for network architectures a and c are linear and cubic functions, respectively.

S2 Effect of Positive Feedback on the *p(luxR)* Promoter

Previous works indicate that *luxR* is capable of positively stimulating transcription from the *p(luxR)* promoter to a small degree [6, 7], thereby resulting in positive feedback on the *p(luxR)* promoter. In contrast, we have assumed that the *p(luxR)* promoter is constitutive. In this section, we numerically explore the effects of this positive feedback.

The experimental results of Sitnikov et al. [7] suggest that the positive feedback from the *p(luxR)* promoter (1.9-fold stimulation) is roughly twenty times less than that from the *p(luxI)* promoter (37-fold stimulation). Consequently, we explore increasing the positive feedback from the *p(luxR)* promoter on network architectures a and b. To do so, we define the amplification factor of promoter j (α_j) as the fold increase in the expression levels due to positive feedback. We consider manipulating the amplification factor for the *p(luxR)* promoter, $\alpha_{p(luxR)} = k_3'/k_4'$, by altering k_4' while leaving k_3' at a constant value. Parameter values are the same as the revised values in Table S3, noting that $k_3' = k_8$ and k_4' is variable.

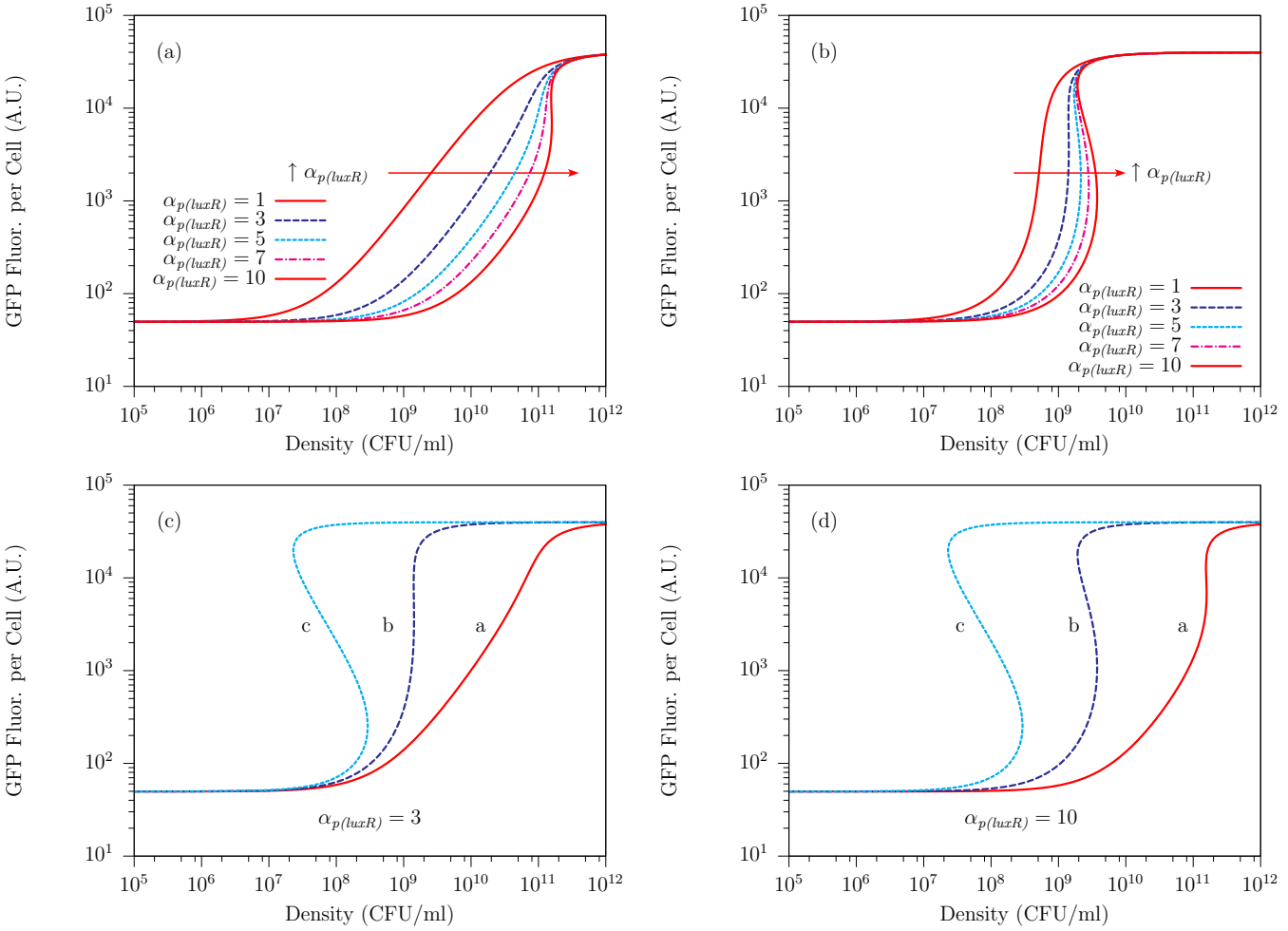

Figure S7: Effect of increasing the amplification factor $\alpha_{p(luxR)}$ for the *p(luxR)* promoter for network architectures a and b. Plot (a): increasing $\alpha_{p(luxR)}$ for network architecture a. Plot (b): increasing $\alpha_{p(luxR)}$ for network architecture b. Plot (c): comparing all three network architectures for $\alpha_{p(luxR)} = 3$. Plot (d): comparing all three network architectures for $\alpha_{p(luxR)} = 10$.

Transcription Factor Binding	Degradation	Cell growth (logistic)
$2\mathrm{R} + 2\mathrm{A} \overset{K_1}{\rightleftharpoons} \mathrm{R}^*$	$\mathrm{R}, \mathrm{A}, \mathrm{G} \overset{k_5, k_6, k_7}{\longrightarrow}$ degraded	$\mathrm{C} \overset{k_9}{\longrightarrow} 2\mathrm{C}$
$\mathrm{R}^* + \mathrm{P}_0 \overset{K_2}{\rightleftharpoons} \mathrm{P}_1$		$r_9 = k_9 c \left(1 - \frac{c}{c_{\max}}\right)$

Architecture a	Architecture b		
$\mathrm{P}_0 \overset{k_4}{\longrightarrow} \mathrm{P}_0 + \mathrm{n_g G}$	$\mathrm{P}_0 \overset{k_4}{\longrightarrow} \mathrm{P}_0 + \mathrm{n_a A} + \mathrm{n_g G}$	*p(luxI)*	Transcription & Translation
$\mathrm{P}_1 \overset{k_3}{\longrightarrow} \mathrm{P}_1 + \mathrm{n_g G}$	$\mathrm{P}_1 \overset{k_3}{\longrightarrow} \mathrm{P}_1 + \mathrm{n_a A} + \mathrm{n_g G}$	*p(luxI)*	
$\mathrm{P}_0 \overset{k_4'}{\longrightarrow} \mathrm{P}_0 + \mathrm{R} + \mathrm{n_a A}$	$\mathrm{P}_0 \overset{k_4'}{\longrightarrow} \mathrm{P}_0 + \mathrm{R}$	*p(luxR)*	
$\mathrm{P}_1 \overset{k_3'}{\longrightarrow} \mathrm{P}_1 + \mathrm{R} + \mathrm{n_a A}$	$\mathrm{P}_1 \overset{k_3'}{\longrightarrow} \mathrm{P}_1 + \mathrm{R}$	*p(luxR)*	

Table S4: Kinetic mechanisms used to model the behaviors of architectures a and b assuming that the *p(luxR)* promoter exhibits positive feedback. Positive feedback from the *p(luxI)* promoter is denoted by the k_3 and k_4 rate constants, while positive feedback from the *p(luxR)* promoter is denoted by the k_3' and k_4' rate constants.

Because the *p(luxI)* promoter has an amplification factor in the model of $\alpha_{p(luxI)} = k_3/k_4 = 200$, we restrict our attention to amplification factors for the *p(luxR)* promoter of $0 \leq \alpha_{p(luxR)} \leq 10$ to account for the experimental observations of Sitnikov et al.[7]. In Figure S7 (a) and (b), we see that the amplification from the *p(luxR)* promoter increases the sharpness of the steady-state quorum-sensing response for both network architectures a and b. Additionally, these figures demonstrate that these values of $\alpha_{p(luxR)}$ maintain the graded and threshold responses of network architectures a and b, respectively. Figure S7 (c-d) compares the steady-state quorum-sensing responses of all three network architectures for the same value of $\alpha_{p(luxR)}$. These two figures demonstrate that increasing the number of *lux* regulatory elements under control of the *p(luxI)* promoter increases the sharpness of the response and reduces the location of the induction threshold for the given set of parameters. Such phenomena result because the positive feedback from the *p(luxI)* promoter is significantly greater than that from the *p(luxR)* promoter.

S3 Effect of Prolonged Quorum-Sensing Induction on Architecture c

Prolonged maximal induction of the quorum-sensing circuit negatively impacts cellular function for the architecture c configuration of pluxRp-101 and pPSSUB-102. As seen in Figure S3, the dynamic fluorescence readings exhibit a weak maximum in intensity, then begin to slowly decrease in value. Determination of cell viability by serial dilution and plating confirms the negative impact on cellular function: Figure S6 (a) demonstrates that the number of viable cells for pluxRp-101 and pPSSUB-102 are consistently lower than those for architectures a and b. Additionally, the plated cells for pluxRp-101 and pPSSUB-102 were consistently smaller than those for architectures a and b (data not shown). Interestingly, pluxRp-103E and pPSSUB-102 only displayed similar effects when exposed to a 3OC6HSL concentration of 1.0 μM (or greater than 100 nM) as shown in Figures S8 and S9. Since over-expression of LuxR, LuxI, and GFPLVA from *p(luxI)* causes such limitations on growth, there is a strong selective pressure to down-regulate the quorum-sensing system. We speculate that the response to this pressure leads to the observed decreases in fluorescence.

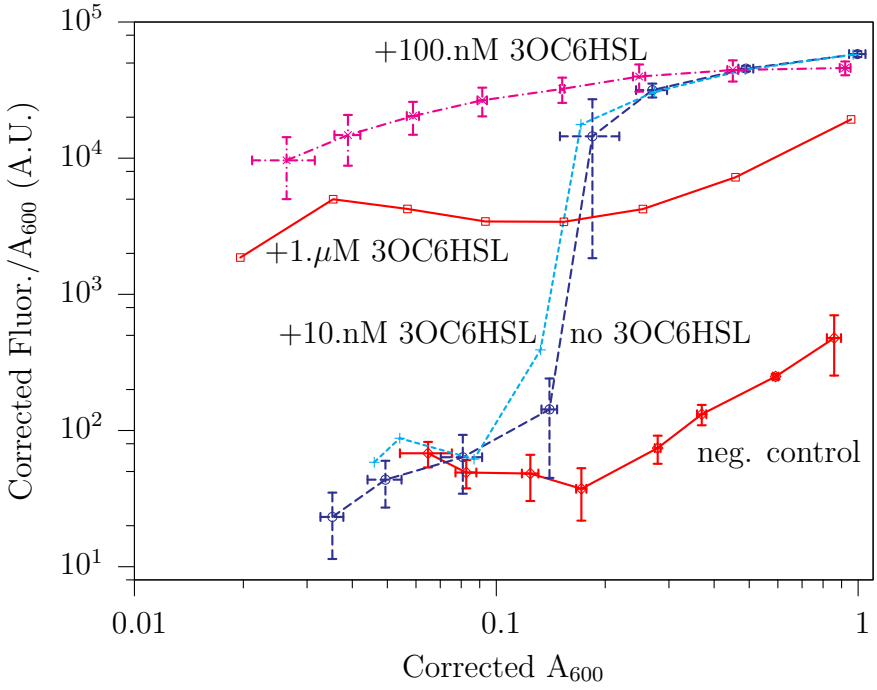

Figure S8: Steady states of pluxRp-103E and pPSSUB-102 as a function of 3OC6HSL induction. The result for the experiment induced at 1.μM 3OC6HSL does not lead to a steady state.

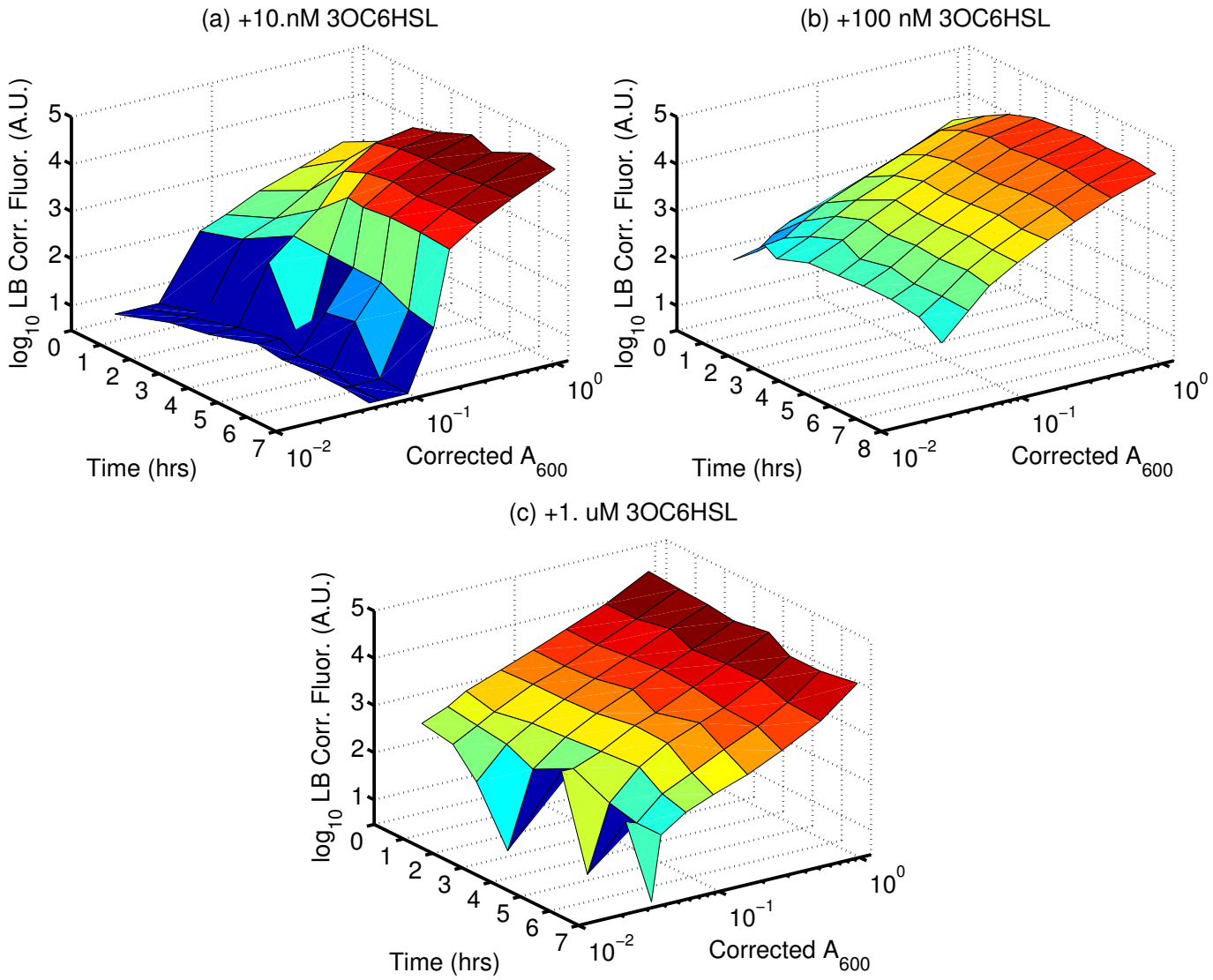

Figure S9: Periodic dilution results for pluxRp-103E and pPSSUB-102 as a function of 3OC6HSL induction. This figure shows the absorbance and fluorescence dynamics over the duration of the periodic dilution experiment. Induction with a 3OC6HSL concentration of 100 nM or lower leads to a stable steady state. Induction with a 3OC6HSL concentration of 1 μM does not achieve a steady state in the duration of the experiment. Each plot uses the same shading to highlight differences in the measured fluorescence values.

References

[1] **Andersen, J. B., C. Sternberg, L. K. Poulsen, S. P. Bjørn, M. Givskov, and S. Molin.** 1998. New unstable variants of green fluorescent protein for studies of transient gene expression in bacteria. Appl. Environ. Microbiol. **64**:2240–2246.

[2] **Bailey, J. E., and D. F. Ollis.** 1986. Biochemical Engineering Fundamentals. McGraw-Hill, New York.

[3] **Basu, S., Y. Gerchman, C. H. Collins, F. H. Arnold, and R. Weiss.** 2005. A synthetic multicellular system for programmed pattern formation. Nature **434**:1130–1134.

[4] **Basu, S., R. Mehreja, S. Thiberge, M.-T. Chen, and R. Weiss.** 2004. Spatiotemporal control of gene expression with pulse-generating networks. Proc. Natl. Acad. Sci. USA **101**:6355–6360.

[5] **Flagan, S., W. Ching, and J. R. Leadbetter.** 2003. *Arthrobacter* strain VAI-A utilizes acyl-homoserine lactone inactivation products and stimulates quorum signal biodegradation by *Variovorax paradoxus*. Appl. Environ. Microbiol **69**:909–916.

[6] **Shadel, G. S., and T. O. Baldwin.** 1991. The *Vibrio fischeri* LuxR protein is capable of bidirectional stimulation of transcription and both positive and negative regulation of the *luxR* gene. J. Bacteriol. **173**:568–574.

[7] **Sitnikov, D. M., G. S. Shadel, and T. O. Baldwin.** 1996. Autoinducer-independent mutants of the LuxR transcriptional activator exhibit differential effects on the two *lux* promoters of *Vibrio fischeri*. Mol. Gen. Genet. **252**:622–625.

[8] **Urbanowski, M. L., C. P. Lostroh, and E. P. Greenberg.** 2004. Reversible acyl-homoserine lactone binding to purified *Vibrio fischeri* LuxR protein. J. Bacteriol. **186**:631–637.